university of groningen

University Medical Center Groningen

University of Groningen

Carbon-supported iron complexes as electrocatalysts for the cogeneration of hydroxylamine and electricity in a NO-H-2 fuel cell

Sheng, Xia; Alvarez-Gallego, Yolanda; Dominguez-Benetton, Xochitl; Baert, Kitty; Hubin, Annick; Zhao, Hailiang; Mihaylov, Tzvetan T.; Pierloot, Kristine; Vankelecom, Ivo F. J.; Pescarmona, Paolo P.

IMPORTANT NOTE: You are advised to consult the publisher's version (publisher's PDF) if you wish to cite from it. Please check the document version below.

Document Version
Final author's version (accepted by publisher, after peer review)

Publication date:
2018

Link to publication in University of Groningen/UMCG research database

Carbon-supported iron complexes as electrocatalysts for the cogeneration of hydroxylamine and electricity in a NO-H₂ fuel cell: a combined electrochemical and Density Functional Theory study.

Xia Sheng[a,b], Yolanda Alvarez-Gallego[c,*], Xochitl Dominguez-Benetton[c], Kitty Baert[d], Annick Hubin[d], Hailiang Zhao[b,e], Tzvetan T. Mihaylov[e], Kristine Pierloot[e], Ivo F. J. Vankelecom[a], Paolo P. Pescarmona[a,f*]

[a] *Centre for Surface Chemistry and Catalysis, University of Leuven (KU Leuven), Celestijnenlaan 200F, 3001 Heverlee, PO Box 2461, Belgium.*

[b] *College of Chemistry, Chemical and Environmental Engineering, Henan University of Technology, Lianhua street 100, P.R. China*

[c] *Separation and Conversion Technology, VITO – Flemish Institute for Technological Research, Boeretang 200, Mol 2400, Belgium*

[d] *Vrije Universiteit Brussel, Research Group Electrochemical and Surface Engineering, Pleinlaan 2, 1050 Brussels, Belgium*

[e] *Department of Chemistry, University of Leuven (KU Leuven), Celestijnenlaan 200 F, 3001 Heverlee, Belgium*

[f] *Chemical Engineering Group, Engineering and Technology institute Groningen (ENTEG),University of Groningen, Nijenborgh 4,9747 AG Groningen, The Netherlands*

* Corresponding authors: p.p.pescarmona@rug.nl; yolanda.alvarezgallego@vito.be

Abstract

Carbon-supported iron complexes were investigated as electrocatalysts for the reduction of nitric oxide (NO) in a H₂-NO fuel cell conceived for the production of hydroxylamine (NH₂OH) with concomitant generation of electricity. Two types of iron complexes with tetradentate ligands, namely

bis(salicylidene)ethylenediimine (Salen) and phthalocyanine (Pc), supported on activated carbon or graphite were prepared and evaluated as electrocatalysts, either without further treatment or after pyrolysis at 700 °C. The performance in the reduction of NO of gas diffusion cathodes based on these electrocatalysts was investigated in an electrochemical half cell (3-electrode configuration) using linear sweep voltammetry (LSV). The most promising electrocatalysts were studied further by chronoamperometric experiments in a H_2-NO fuel cell, which allowed comparison in terms of power output and hydroxylamine production. Depending on the concentration of the NO feed (6 or 18%), the best electrocatalytic performance was delivered either by FePc or FeSalen. The gas diffusion electrode based on FeSalen supported on activated carbon with 0.3 wt% Fe-loading provided the highest current density (86 A/m^2) and the best current efficiency (43%) towards the desired NH_2OH when operating at the higher NO concentration (18%). Moreover, FeSalen offers the advantage of being cheaper than FePc. The experimental work was complemented by density functional theory (DFT) calculations, which allowed to shed more light on the reaction mechanism for the reduction of nitric oxide at the atomistic level.

1. Introduction

Hydroxylamine (NH_2OH) is an important bulk chemical. Its main industrial application is in the form of hydroxylammonium sulphate ($NH_3OH)_2SO_4$, as intermediate in the synthesis of ε-caprolactam for the production of Nylon-6.[1] The main route for the industrial production of NH_2OH is the catalytic hydrogenation of nitric oxide (NO), with platinum on activated carbon (Pt/C) being the most effective catalyst for this reaction.[2] An attractive and sustainable alternative to conventional chemical processes for

exergonic redox reactions consists in splitting the reaction in two half reactions that are carried out in a fuel cell set-up.[3] This approach, typically referred to as electrochemical cogeneration, would allow coupling the production of a useful chemical to the generation of electricity.[4-8] If this approach is applied to the synthesis of hydroxylamine in a H_2-NO fuel cell,[9, 10] the anodic reaction is the oxidation of molecular hydrogen, whereas various reactions can occur competitively at the cathode:

Anode: $H_2 \rightarrow 2H^+ + 2e^-$ $E^0 = 0.0$ V   (1)

Cathode: $2NO + 2H^+ + 2e^- \rightarrow N_2O + H_2O$ $E^0 = 1.59$ V   (2)

$2NO + 4H^+ + 4e^- \rightarrow N_2 + 2 H_2O$ $E^0 = 1.68$ V   (3)

$NO + 3H^+ + 3e^- \rightarrow NH_2OH$ $E^0 = 0.38$ V   (4)

$NO + 5H^+ + 5e^- \rightarrow NH_3 + H_2O$ $E^0 = 0.73$ V   (5)
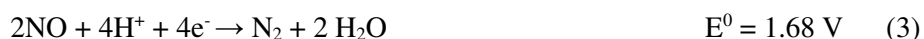
The selectivity towards NH_2OH strongly depends on the potential at which the fuel cell is operated and on the nature of the electrocatalyst employed in the cathode. In general, N_2O is obtained at higher cell potential, whereas NH_2OH formation is predominant at lower cell potential, with other compounds such as N_2 and NH_3 (electrochemical route) or HNO_2 and N_2O (chemical route) as possible by-products.[9, 10] In order to make this electrochemical route applicable for the selective synthesis of NH_2OH, it is vital to develop a suitable electrocatalyst in terms of cost, NO conversion and selectivity towards NH_2OH. The first generation of electrocatalysts for the electrochemical reduction of NO were based on noble metal nanoparticles [9-13] or on macrocyclic transition metal complexes.[14, 15] Pt and Pd-based electrocatalysts yield relatively large current densities but they typically display low selectivity towards NH_2OH, due to the preferential formation of NH_3 and N_2O as products.[15, 16] NH_3 is generated by the further reduction of NH_2OH, whereas the formation of N_2O is associated to the presence of neighbouring metal atoms at the surface of the electrocatalyst, which can promote the interaction of two NHO intermediates leading to the formation of N_2O and H_2O.[15] Higher hydroxylamine selectivity was achieved employing electrocatalysts based on macrocyclic transition metal complexes. The increased selectivity was ascribed to the large distance between the metal centres belonging to two adjacent complexes.[14, 15] Within this class of

3

electrocatalysts, iron-phthalocyanine (FePc, see Fig. 1), cobalt-phthalocyanine (CoPc), cobalt-porphyrin (CoPor) and vitamin B12 have been reported. FePc on activated carbon (FePc/AC) or graphite (FePc/Gr) displayed the most promising performances with selectivity up to 90% for NH_2OH.[10, 14, 15] Recently, some of us reported a novel class of electrocatalysts for the reduction of NO to NH_2OH, consisting of iron-containing N-doped carbon materials derived from activated carbon and polyaniline incorporating Fe sites.[8] These electrocatalysts proved much superior compared to FePc/AC in terms of selectivity towards NH_2OH, power generation and NH_2OH production rate when employing a gas feed with high NO concentration (18%).

In this work, we studied for the first time electrocatalysts based on the readily available and relatively inexpensive complex of Fe with N,N'-bis(salicylidene)ethylenediimine (FeSalen, Fig. 1) for the electrochemical reduction of NO to NH_2OH. Fe-sites are suitable for promoting the electrocatalytic reduction of NO to NH_2OH because iron has two accessible oxidation states (II and III), which allows transferring an electron from Fe^{2+} to NO upon its adsorption on the metal centre. Both Salen and Pc form tetradentate complexes with iron cations, but in Salen complexes the metal is coordinated to the ligand through metal-2N2O interactions, whereas in Pc complexes the metal is coordinated through metal-4N interactions. Moreover, in phthalocyanine the π-delocalisation spans over the whole ligand, while it is less extended in Salen (Fig. 1). Both the nature of the atoms coordinating the iron cations and the extension of the π-delocalisation of the ligand coordinating to Fe are expected to influence the strength of the adsorption of NO onto the Fe centre and, consequently, affect the electrocatalytic activity and the selectivity of the supported complex. However, it is difficult to predict the extent of this effect and whether a stronger adsorption would be favourable or detrimental for the catalytic activity, as the activity of (electro)catalysts as a function of adsorption energy is generally described by a volcano curve with a maximum at intermediate adsorption strength.[17] For their application as electrocatalysts, the metal complexes are typically supported on an electrically conductive carbon material. In this context, the smaller size of FeSalen compared to FePc is an asset, as it would allow reaching higher Fe-content in a hypothetical material consisting of a monolayer

of the metal complex adsorbed onto the carbon support. In this work, the FeSalen complex was supported onto two types of conductive carbon materials: activated carbon (FeSalen/AC) and graphite (FeSalen/Gr). The activated carbon was selected as support because of its high specific surface area, whereas graphite was chosen for its high conductivity and stability. FePc/AC was also prepared and used as reference electrocatalyst. Besides high activity and selectivity, an optimum electrocatalyst should display high stability under the operating conditions. This can represent a challenge in the reduction of NO to NH_2OH, as the fuel cell typically employs 3M H_2SO_4 as electrolyte (with the purpose of stabilising the formed NH_2OH in the form of $(NH_3OH)_2SO_4$). Metal complexes are soluble in concentrated acidic solutions and, therefore, would tend to leach from the support, leading to deactivation of the electrocatalyst. A pyrolysis treatment was investigated to improve the stability of the supported FeSalen and FePc complexes against leaching, though this would occur at the cost of deterioration of the structure of the organic ligand.[18] The series of electrocatalysts described above was integrated in gas diffusion electrodes (GDEs) and tested as cathodes for the reduction of NO by linear sweep voltammetry (LSV) in a cathode half-cell set-up, and by chronoamperometry in a NO-H_2 fuel cell with two different concentrations of NO in the gas feed.[19] This experimental study was complemented by density functional theory (DFT) calculations of the reaction pathway for the NO reduction to NH_2OH over a Fe-complex. Previous experimental and theoretical work suggested that isolated metal centres, like those in FePc, are the active sites for the reduction of NO to NH_2OH.[14-16, 20, 21] However, the mechanism of the reduction of NO over this kind of transition metal complexes is not yet fully understood. [22-24]. Here, we propose a complete reaction pathway for the NO reduction to NH_2OH based on DFT modelling of possible reduction steps at the axial coordination site of a ferrous porphyrin (FePor) complex. These DFT calculations provide information about the stability of the reaction intermediates which is hardly obtainable by other means, thus offering a useful support to interpret the experimental electrocatalytic results.
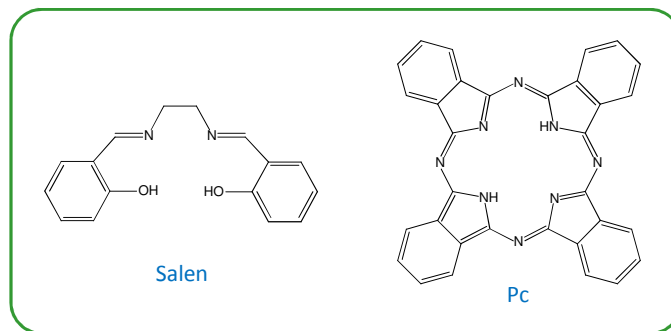
Figure 1. Chemical structure of the ligands used to prepare the supported iron complexes employed as electrocatalysts: N,N'-bis(salicylidene)ethylenediimine (Salen, left) and phthalocyanine (Pc, right).

2. Experimental

2.1 DFT computational procedure

DFT calculations were carried out with the Turbomole 6.3/6.4 package.[25] The molecular geometries of iron-porphyrin (FePor) and the related five-coordinated model complexes, FePor-L (where L = NO, NHO, NOH, N(H)OH, NH_2O, NH_2OH, N(H)(OH)NO, NH_2, NH_3, NH_2NO), were optimised for the lowest-lying spin states utilising the BP86 functional,[21, 26] combined with the ecp-10-mdf/ecp-10-mdf pseudopotential/valence basis set (with one f primitive (2.0 exponent))[16] for Fe and 6-31G(d) basis sets for the rest of the elements. Frequency calculations were performed to ensure that the optimised structures are minima on the potential energy surface and to obtain the thermochemical data. Furthermore, single point B97-D calculations[27] with more extended basis sets, *i.e.* def2-TZVP[28] for all atoms, were carried out on the BP86 optimised structures. The advantage of using the B97-D functional is that it has been parameterised for accurate description of dispersion interactions (van der Waals effects), which give a significant contribution to the binding energy of small molecules (*e.g.* NO) to FePor.[29] The unrestricted DFT formalism was used in all cases.

The electrochemical reactions were modelled according to the strategy proposed by Nørskov et al.[17, 30], in which the chemical potential for the reaction ($H^+ + e^-$) can be related to that of 1/2 H_2 in the gas-phase by setting the potential (E) of a standard hydrogen electrode as reference. Thus, at standard conditions where E

= 0 V, pH = 0, p = 1 bar and T = 298.15 K, the relative free energy for the reaction L + H$^+$ + e$^-$ → LH can be approximated by the free energy change of the simplified reaction L + 1/2H$_2$ → LH. Based on this, for each electrochemical step the reaction energy is obtained from the DFT gas-phase Gibbs free energies as follows:

$$\Delta_r G = \sum_{prod.} G - \sum_{reag.} G \tag{6}$$

where G was estimated as the sum of the B97-D calculated electronic energy, the zero-point energy and the thermal contributions to the free energy in the gas-phase (T = 298.15 K and p = 1 bar). The latter two terms were obtained at the level of theory used for geometry optimisation employing the rigid rotor-harmonic oscillator approximation without scaling.

The binding energy of each ligand (L) to the FePor is calculated as:

$$\Delta G = G(L) + G(FePor) - G(FePor\text{-}L) \tag{7}$$

By convention, a positive binding energy indicates a bound state.

2.2 Synthesis of the electrocatalysts

FeSalen was prepared according to previously reported methods [31, 32], as described in more detail in the Supporting Information. Iron (II) phthalocyanine (FePc, >95%) was purchased from TCI Europe. Activated carbon (AC, Norit® SX1G) and graphite (Gr, from Sigma-Aldrich) were washed with 6 M HCl at room temperature for 24 h to remove impurities. Then, FeSalen was supported on each carbon material by dissolving the selected amount of complex (0.26 g) in dichloromethane, followed by addition of 15 g activated carbon or graphite, and by stirring under reflux for 24 h. Next, the solvent was removed in a rotary evaporator. The resulting material was purified by Soxhlet extraction with dichloromethane for 16 h. Finally, the solid was dried in an oven for 13 h at 120 °C under reduced pressure. The obtained samples were named, following their theoretical metal loading, as FeSalen$_{(0.3)}$/AC and FeSalen$_{(0.3)}$/Gr. The pyrolysed samples were

prepared by thermal treatment in a quartz tubular oven under N_2 for 7 h (flow rate: 1 ml s^{-1}) at 700 °C, with a heating rate of 3°C min^{-1}, and denoted as FeSalen$_{(0.3)}$/AC-pyr and FeSalen$_{(0.3)}$/Gr-pyr. FePc was supported on AC by dissolving FePc (0.45 or 4.5 g) in concentrated aqueous H_2SO_4 (98%, 5 ml), followed by sonication for 30 min [33] and by addition of 15 g of AC (while sonicating). The suspension was then washed with deionised water until pH = 7. The solid was removed by filtration and dried at 70 °C in an oven overnight. The resulting materials are denoted as FePc$_{(0.3)}$/AC and FePc$_{(3.0)}$/AC. An aliquot of these samples was subjected to pyrolysis (procedure as for FeSalen), and denoted as FePc$_{(0.3)}$/AC-pyr and FePc$_{(3.0)}$/AC-pyr.

2.3 Physicochemical characterisation

^{1}H-NMR spectra were recorded on a Bruker Advance 300 MHz spectrometer, using deuterated chloroform (CDCl$_3$) as the solvent, and were analysed using the SpinWorks 3.1.7 software. FT-IR spectra of the metal complexes (as-such and supported) were measured in the range 400-4000 cm^{-1} on a Biorad FTS 155 spectrometer (using KBr pellets). The Fe-content of the supported complexes was evaluated by X-ray fluorescence (XRF, XLAB-2000 and XEPOS HE, Spectro) under He atmosphere, and by inductively coupled plasma optical emission spectroscopy (ICP-OES) carried out on a Perkin Elmer Optima 3300DV. The percentages of C and N were determined by using the Dumas-method on a Vario Max CN analyser (Elementar).[34] Surface areas and micropore volumes were determined by N_2 adsorption at 77 K (t-method) on a Micromeritics Tristar 3000, and evaluated with the application of the Brunauer-Emmett-Teller (BET) and Dubinin-Radushkevich (DR) equations. Room-temperature Raman spectra were measured on a LabRAM HR Evolution-Horiba Scientific system with a green laser (λ = 532 nm).

2.4 Electrochemical characterisation

Electrochemical measurements were performed at room temperature using previously reported set-ups[19], which are described in more detail in the Supporting Information.

The current efficiency towards NH$_2$OH [CE$_{NH_2OH}$(%)] and the yield of NH$_2$OH [Y$_{NH_2OH}$(%)] were calculated according to the following expressions:

$$CE_{NH_2OH}\ (\%) = \frac{mol_{NH_2OH}(exp)}{mol_{NH_2OH\ max}(calc)}\ 100\% \qquad (8)$$

$$mol_{NH_2OH\ max}(calc) = \frac{Q}{n*F} \qquad (9)$$

$$Y_{NH_2OH}\ (\%) = \frac{mol_{NH_2OH}(exp)}{mol_{NO}(input)}\ 100\% \qquad (10)$$

where mol_{NH_2OH} (exp) is the moles of NH$_2$OH produced in the experiment, as determined by potentiometric titration of (NH$_3$OH)$_2$SO$_4$ [which was generated by reaction of the formed hydroxylamine with the liquid electrolyte (3M aqueous H$_2$SO$_4$) – see Supporting Information; mol_{NH_2OH} (exp) = 2 $mol_{(NH_3OH)_2SO_4}$(exp)];
$mol_{NH_2OH\ max}$(calc) is the maximum number of moles of NH$_2$OH that could be obtained in the experiment, as calculated according to equation (9) from the charge that passed through the cathode over the whole duration of the experiment (Q, in Coulomb), the moles of the electrons exchanged per mol of NH$_2$OH produced ($n = 3$ for NO + 3H$^+$ + 3e$^-$ → NH$_2$OH) and the constant of Faraday (F = 96485 C mol^{-1}); mol_{NO}(input) is the moles of NO that were fed to the cathode for the whole duration of the experiment, as calculated from the total time of the experiment, the volumetric flow of gas feed and the concentration of NO in the gas feed. The production rate ($mol_{NH2OH} \cdot h^{-1} \cdot m^{-2}$) represents the moles of NH$_2$OH produced per hour and per m^2 of cathode.

2.5 Leaching tests

Leaching tests were performed to determine the stability of the electrocatalysts in the electrolyte solution used in the electrochemical tests. The electrocatalyst powder (FePc$_{(0.3)}$/AC and FePc$_{(0.3)}$/AC-pyr, 0.5 g of each) was suspended in 10 ml of 3M aqueous H$_2$SO$_4$. The mixtures were placed in tightly capped glass bottles wrapped with aluminium foil and shaken on a rotating mixer at 25°C. Both samples were kept in the acidic solution for 52 h; the pyrolysed sample was also treated for 168 h. Next, the liquid was separated from

the solid by centrifugation and the solid was analysed by ICP-OES to measure the metal loading (Fe wt%).

The percentage decrease of Fe-content in the catalyst powder was calculated as:

$$Fe \; leaching \; (\%) = \frac{[(Fe \; wt\%)_{final} - (Fe \; wt\%)_{initial}]}{(Fe \; wt\%)_{initial}} \quad (11)$$

In addition, the Fe-content (wt%) in $FePc_{(0.3)}$/AC-pyr after 130 h of electrode operation was determined by XRF.

3. Results and discussion

The electrochemical reduction of NO to produce NH_2OH over supported Fe-complex electrocatalysts was studied by combining experimental work and DFT calculations. The theoretical study is presented first, as it provides a useful basis for the discussion of the results of the experimental investigation. Then, the synthesis and characterisation of the electrocatalysts are presented and discussed, followed by the evaluation of their performance in the reduction of NO to NH_2OH by LSV in a cathode half-cell set-up, and by chronoamperometry in a NO-H_2 fuel cell.

3.1 DFT study of the reduction of nitric oxide over Fe-complexes

In order to investigate the reaction pathways for the reduction of NO over Fe-complexes, a theoretical study by means of the density functional theory (DFT) was carried out. As a model system we chose a Fe-complex of the widely studied macrocyclic porphyrin (Por) 4N-ligand,[29, 36] which is smaller but structurally related to the Pc ligand used in the experimental part of this work. For the electrochemical reduction of NO to NH_2OH, the parent compound needs to acquire three H atoms (as $H^+ + e^-$) in a stepwise process, whereas the complete reduction to NH_3 (+ H_2O) requires five ($H^+ + e^-$) in total. At each reaction step, more than one intermediate might be formed by the addition of a H atom, depending on the site at which the

addition occurs (N or O). Moreover, most of these intermediates can potentially react also with another NO molecule, leading to a range of competitive reaction paths with different final products. The paths leading to the most stable intermediates (as indicated by DFT calculations) and to the four possible products of the electrochemical reduction of NO (N_2O, N_2, NH_2OH and NH_3) are illustrated in Fig. 2. The free energy profile of the reaction pathways together with the corresponding FePor-L binding energies are presented in Fig. 3. Selected structural parameters and relative energies of all intermediates in their different spin multiplicities can be found in Table S1 in the Supporting Information (SI), whereas the Cartesian coordinates of the iron-porphyrin model systems in their ground state are provided in Table S2. Here, only the relative energies corresponding to the lowest-energy spin states of these species are presented and discussed. It should be noted that the proposed reaction paths and the corresponding energy profile in Fig. 2 and 3 are spin conserving, *i.e* with spin changes of at most ± ½ in each step.
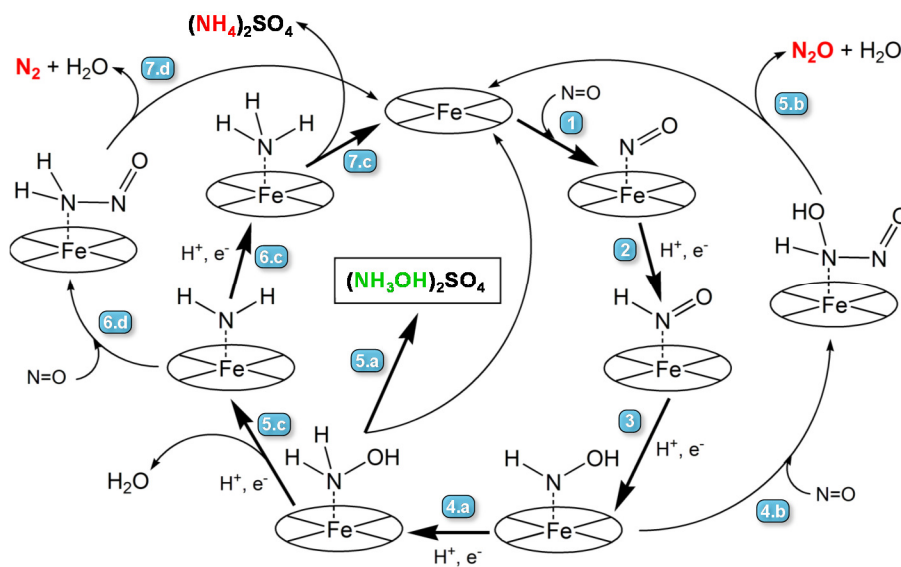

Figure 2. Proposed reaction paths for the reduction of NO catalysed by Fe-complexes.
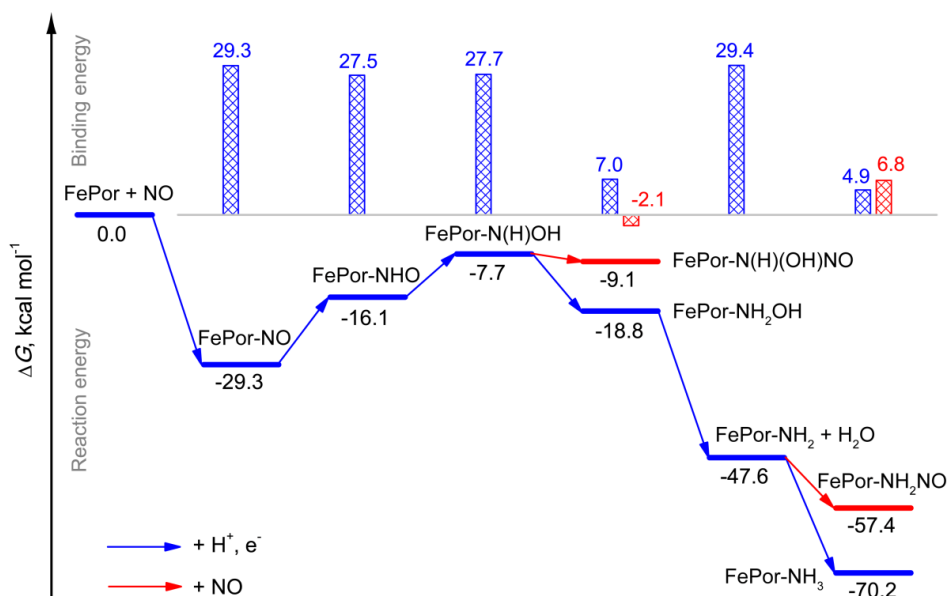
Figure 3. Free energy profile for the reduction of NO over a FePor catalyst and the FePor-L binding energies (L = NO, NHO, N(H)OH, NH$_2$OH, N(H)(OH)NO, NH$_2$, NH$_3$, NH$_2$NO). All values are in kcal mol^{-1}.

The ground state of the FePor is a triplet (S = 1) with two unpaired electrons in the Fe 3d$_{xz}$ and 3d$_{yz}$ orbitals.[37] NO is a free radical with one unpaired electron. The first step of the electrocatalytic NO reduction is its addition to the Fe-complex (step 1 in Fig. 2). NO binds to the metal via the N-atom to form a ferrous nitrosyl Fe-N-O (formation of isonitrosyl Fe-O-N complex or bridging nitrosyl are unlikely as these were found to be metastable states [38, 39]). The Fe-NO bond formation involves a strong covalent π-interaction between the Fe (3d$_{xz}$, 3d$_{yz}$) and the NO π* orbitals, resulting in a delocalised set of bonding and anti-bonding molecular orbitals: (d$_{xz,yz}$-π$_{x,y}$*)$_b$ and (d$_{xz,yz}$-π$_{x,y}$*)$_a$. The formation of FePor-NO is exergonic, with an estimated value of -29.3 kcal mol^{-1}. It can be assumed that in the resting state (*i.e.* in the absence of NO in the reaction system) the FePor catalyst exposed to water might contain a coordinated H$_2$O molecule at its axial position.[40] The FePor-OH$_2$ binding energy, however, was found to be rather small (< 1 kcal mol^{-1}), which means that the H$_2$O ligand can be replaced very easily by NO. In the second step, (H$^+$ + e$^-$) addition to either the N or the O atom of the NO fragment may occur. The FePor-N(OH) complex is much higher in

energy (~14 kcal mol^{-1}) than the FePor-N(H)O complex. Therefore, only the FePor-N(H)O intermediate is considered in the reaction scheme (step 2). This step is endergonic and requires 13.2 kcal mol^{-1}. In the third step, FePor-N(H)O is reduced to either FePor-NH$_2$O or FePor-N(H)OH. As the latter is more stable by 3 kcal mol^{-1}, FePor-NH$_2$O is not included in the reaction scheme. The free energy demand for the reduction of FePor-N(H)O to FePor-N(H)OH (step 3) is 8.4 kcal mol^{-1}. Next, the FePor-N(H)OH complex can be further reduced to FePor-NH$_2$OH, with an energy gain of 11.1 kcal mol^{-1} (step 4.a). From Fig. 3 it can be seen that the binding energies of N(H)OH and NHO to FePor are comparable to the binding energy of NO, indicating that these species would not tend to detach from the catalytic site until a NH$_2$OH molecule is formed. On the other hand, the FePor-NH$_2$OH binding energy obtained from DFT is only 7.0 kcal mol^{-1}. Accordingly, a relatively large Fe-N bond length (about 2.2 Å) is predicted for FePor-NH$_2$OH. Such a weak bond may be broken easily, also considering that the dissociated NH$_2$OH fragment would be stabilised as NH$_3$OH$^+$ by the strongly acidic reaction environment and the formation of (NH$_3$OH)$_2$SO$_4$ (step 5.a). Hence, at the FePor-NH$_2$OH stage of the reduction process, the release of NH$_2$OH can occur with a possible replacement by an incoming NO molecule. This path is in competition with the further reduction of FePor-NH$_2$OH to FePor-NH$_2$ (+ H$_2$O), and finally to FePor-NH$_3$ (steps 5.c and 6.c). These two steps are exergonic and successively lower the energy by 28.8 and 22.6 kcal mol^{-1}, respectively. Which of these processes will dominate depends on external factors, such as the acidity of the medium or the cell potential. The free energy changes of the reduction processes in Fig. 3 refer to standard conditions (E = 0 V, pH = 0, p = 1 bar and T = 298.15 K). By increasing E by *e.g.* 0.1 V, each of these processes would become more favourable by a free energy value of 2.3 kcal/mol.[17] Therefore, an increase in the cell potential is expected to have a negative effect on the selectivity towards NH$_2$OH, as it would promote the competing reduction step of FePor-NH$_2$OH to FePor-NH$_2$ + H$_2$O, while leaving the FePor-NH$_2$OH binding energy unaffected. The NH$_2$ ligand produced in the reduction step is strongly bound to FePor, which is a good premise for its electrocatalytic reduction to the end product NH$_3$. With a binding energy of only 4.9 kcal mol^{-1} and a long Fe-N bond distance of 2.3 Å, the

bound NH_3 can easily detach from the surface (as $(NH_4)_2SO_4$, step 7.c), thus leaving a free catalytic site for a new NO molecule.

As mentioned above, any of the Fe-bound species in Fig. 3 could in principle also react with a second NO molecule, leading to the formation of side products (N_2O and N_2). The detailed investigation of all these possible side reactions is outside the scope of this study. Here, we focus only on the two stages of the reduction process in which the formation of these side products is most likely, *i.e.* from the FePor-N(H)OH and FePor-NH$_2$ intermediates. Both these molecules have an $S = 1/2$ ground state. Formally, they could be considered as Fe(III) ($S = 1/2$) coordinated to a closed-shell N(H)OH$^-$ or NH$_2^-$. However, plots of the spin density in both molecules show that the unpaired electron is delocalised over the Fe-N bond (Fig. S1 in the SI). In both cases, the ligand has partial radical character, thus making it susceptible to attack by a second NO radical. The reaction of FePor-N(H)OH with NO to give FePor-N(H)(OH)NO (step 4.b) and that of FePor-NH$_2$ to yield FePor-NH$_2$NO (step 6.d) are both exergonic (Fig. 3). Moreover, in both products the bond between FePor and the axial ligand is very weak. In the case of N(H)(OH)NO, the DFT binding energy (gas phase) is even slightly negative (Fig. 3). Therefore, the formation of these products should be followed by the immediate dissociation from the FePor moiety. The most probable fate of the free molecules involves a series of intramolecular proton transfers: N(H)(OH)NO can convert to HON=NOH (hyponitrous acid), which can then decompose into $N_2O + H_2O$ (step 5.b in Fig. 2), whereas NH$_2$NO can generate $N_2 + H_2O$ (step 7.d).[41, 42] The DFT calculations also indicate that these side reactions with NO are less favourable than the competitive reduction processes, leading to NH_2OH and NH_3 respectively (Fig. 3). Based on these data and taking into consideration that the formation of N_2O or N_2 requires two NO molecules in each case, it is expected that these side products will be formed in minor amounts at low NO concentrations. However, high NO concentrations should promote the formation of N_2O and N_2, resulting in lower selectivity towards the desired NH_2OH product.

In summary, the qualitative reaction scheme based on DFT calculations suggests that the formation of hydroxylamine (as NH_3OH^+) will compete with that of ammonia (as NH_4^+), whereas N_2O and N_2 are expected to be minor side products when low NO concentration is employed.

Based on these DFT calculations, it was also possible to estimate the enthalpy change and the Gibbs free energy change associated with the reaction $NO + 3/2\ H_2 \rightarrow NH_2OH$ (at standard conditions) as -99.6 and -49.4 kJ mol^{-1}, respectively. The latter corresponds to $E^0 = 0.17$ V, which is significantly lower than the previously reported value, 0.38 V. However, the two values are not directly comparable because the calculations were carried out in gas phase while the standard potential refers to reaction in solution.

3.2 Synthesis and characterisation of the supported Fe-complexes

The performance of supported iron complexes as electrocatalysts for the reduction of nitric oxide to hydroxylamine is expected to depend on a combination of physicochemical properties: the nature of the metal, the structure of the metal complex, the metal loading and the features of the material used as support. In this work, Fe-complexes (FeSalen and FePc) were supported onto a carbon material (activated carbon or graphite) with a 0.3 wt% Fe-loading (and at 3.0 wt% for FePc/AC). These materials, as such or after a pyrolysis treatment, were used as electrocatalysts for the reduction of NO to NH_2OH. The successful adsorption of the metal complexes on the support was proven by the values of Fe-content obtained from XRF and ICP-OES (Table 1), which are in excellent agreement between the two techniques and with the theoretical values for the samples with 0.3 wt% of Fe on AC. For the material with higher metal loading (3.0 wt%), XRF tended to underestimate the Fe-content compared to ICP-OES, which was again in good agreement with the theoretical values. For the samples supported on graphite, the Fe-loading was higher than the theoretical value, probably due to loss of some of the graphitic material during the adsorption and washing procedure. In all cases, the pyrolysis treatment did not affect the metal loading substantially.

Table 1. Metal contents of the synthesised electrocatalysts.

Electrocatalyst	Fe-loading (wt%)		
	theoretical	measured (XRF)	measured (ICP-OES)
FePc$_{(0.3)}$/AC	0.30	0.30	0.32
FePc$_{(0.3)}$/AC-pyr	0.30	0.31	0.28
FePc$_{(3.0)}$/AC-pyr	3.0	2.2	3.2
FeSalen$_{(0.3)}$/AC	0.30	0.29	0.30
FeSalen$_{(0.3)}$/AC -pyr	0.30	0.24	0.27
FeSalen$_{(0.3)}$/Gr	0.30	0.49	n.a.
FeSalen$_{(0.3)}$/Gr-pyr	0.30	0.55	n.a.

n.a. = not analysed

The supported Fe-complexes were also studied by FT-IR spectroscopy (Fig. 4). The spectrum of the unsupported FePc complex shows characteristic bands of the benzo-fused pyrrole ring (isoindole) of phthalocyanine at 1422, 1322, 1278, 1166, 1116, 1078 and 722 cm^{-1} (Fig. 4.A).[43, 44, 45] The strong bands at 1006-1008 cm^{-1} and 1539 cm^{-1} that are characteristic of the non-coordinated Pc, are absent in the FT-IR spectrum of FePc, suggesting that the sample contains no (or negligible amounts of) free ligand.[44] According to the literature, the metal-ligand (Fe-N) vibration bands are observed in the 888-919 cm^{-1} range.[45] The signal appearing at 892 cm^{-1} indicates the coordination bonds of Fe with the four surrounding nitrogen atoms in the pyrrole rings. The main characteristic peaks of FePc can be observed also in the spectrum of FePc$_{(3.0)}$/AC, confirming the successful adsorption of the complex on the carbon support. The peak positions are virtually not altered by the adsorption, which points towards a weak interaction between the metal complex and the activated carbon support.[45] For the sample with lower FePc loading (FePc$_{(0.3)}$/AC), the peaks originating from the complex become hard to detect. The spectra of the supported metal complexes also display characteristic signals originating from the activated carbon support.[46, 47] The main absorption band observed in the spectrum of the untreated activated carbon at 1634 cm^{-1}, which is clearly visible also in the spectra of FePc$_{(3.0)}$/AC, FePc$_{(0.3)}$/AC and FePc$_{(0.3)}$/AC-pyr (Fig. 4.A), is generally assigned to aromatic ring stretching in activated carbon or to stretching vibration of surface C=O groups,[48]

though a contribution of the bending mode of adsorbed water cannot be excluded.[49, 50] The signal at 875 cm^{-1} is attributed to out-of-plane bending vibration of C–H in deformed benzene rings after the acidic treatment of the activated carbon with HCl (see Experimental section).[51, 52] The broad signals in the 3200-3500 cm^{-1} region are attributed to the stretching vibration of O–H groups (from surface alcohol groups and adsorbed H$_2$O).[44, 53]

The FT-IR spectrum of the unsupported FeSalen complex (Fig. 4B) shows characteristic signals at 1623, 1603, 1531, 1448, 1384 , 1272 and 754 cm^{-1}.[54-56] The characteristic C=N peak at 1635 cm^{-1} of the free Salen ligand is not observed, confirming the complexation of the iron cation.[55] The most intense among the FeSalen-signals are also observed in the spectrum of the supported complex (FeSalen$_{(0.3)}$/AC), though with lower intensity, confirming that the metal complexes were successfully supported on the carbon material. The signals due to the activated carbon support in the 3200-3500 cm^{-1} region, at 1634 cm^{-1} and 875 cm^{-1} (*vide supra*), are also clearly observed in this spectrum (Fig. 4.B). During the pyrolysis process, the chemical structure of the metal complex is significantly deteriorated, as evidenced by the nearly complete disappearance of the peaks due to the FeSalen complex in the FT-IR spectrum of FeSalen$_{(0.3)}$/AC-pyr.[57]
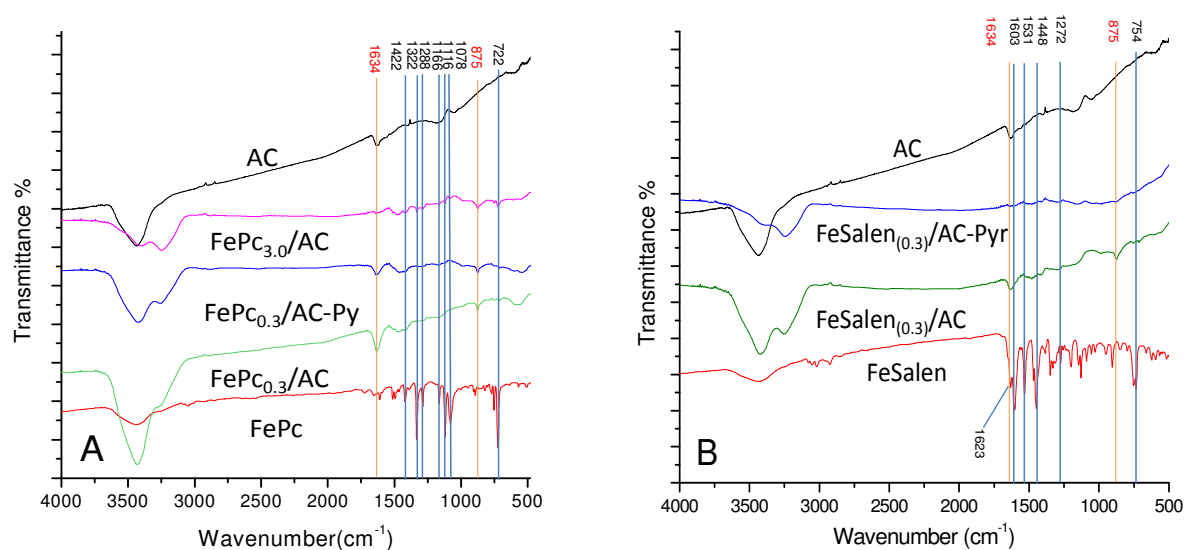

Figure 4. FT-IR spectra of: (A) the supported FePc electrocatalysts, compared to unsupported FePc and to the AC support; (B) the supported FeSalen electrocatalysts, compared to unsupported FeSalen and to the AC support.

Raman spectroscopy provided information about the species constituting the carbon framework of the electrocatalysts. The G-band at 1604 cm^{-1} stems from sp^2 C atoms in the bulk of graphite layers, whereas the D-band at 1330 cm^{-1} corresponds to defects and disordered structures (Fig. 5).[58] Therefore, the ratio between the areas of these two peaks (A$_D$/A$_G$) gives an indication of the overall order and degree of graphitisation in carbon structures. The two less intense signals at 1200 and 1510 cm^{-1} found by deconvoluting the Raman spectrum are associated with carbon atoms outside a perfectly planar graphitic layer and to five-membered rings or heteroatoms integrated into the aromatic structure.[18] The A$_D$/A$_G$ values for the pyrolysed and non-pyrolysed FeSalen$_{(0.3)}$ supported on activated carbon are the same (A$_D$/A$_G$ = 2.29) and are also very similar to that of the parent activated carbon (A$_D$/A$_G$ = 2.23). These results indicate that the pyrolysis treatment at 700 ºC did not significantly affect the chemical structure of the carbon support.
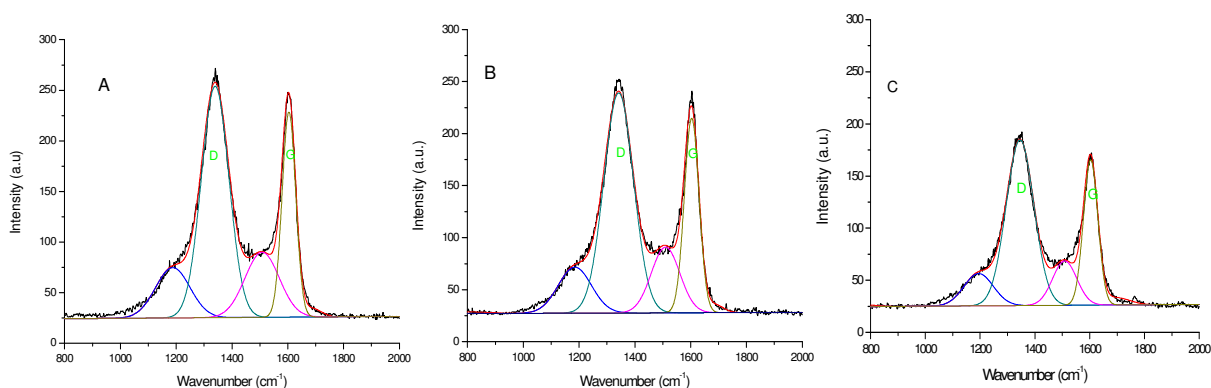

Figure 5. Raman spectra (with deconvolution) of: (A) FeSalen$_{(0.3)}$/AC; (B) FeSalen$_{(0.3)}$/AC-pyr and (C) AC.

The BET specific surface area and pore volume of selected active layers (consisting of 90 wt% electrocatalyst and 10 wt% of PTFE) were determined by N$_2$-physisorption (Table 2). The adsorption of 0.3 wt% Fe as FePc or FeSalen on activated carbon does not affect significantly the surface area of the material. On the other hand, the surface area and pore volume increase slightly upon pyrolysis. This behaviour is ascribed to the decomposition of oxygenated functional groups that are typically present on the surface of the porous activated carbons.[59]

Table 2. Specific surface area and pore volume of the active layer of the GDEs, as a function of the nature of the electrocatalyst used in the active layer.

Electrocatalyst in the active layer	S_{BET} (m^2 g^{-1})	Pore volume (cm^3 g^{-1})
AC	549	0.42
FePc$_{(0.3)}$/AC	555	0.45
FeSalen$_{(0.3)}$/AC	559	0.48
AC-pyr	613	0.49
FePc$_{(0.3)}$/AC-pyr	603	0.48
FeSalen$_{(0.3)}$/AC-pyr	601	0.49

In summary, the physicochemical characterisation of the electrocatalysts demonstrated the successful deposition of Fe-complexes onto the carbon supports, and suggested that neither the adsorption of the complex nor pyrolysis have a major impact on the physicochemical properties of the carbonaceous support.

3.3 Supported FeSalen electrocatalysts for the reduction of NO (half-cell tests)

A preliminary assessment of the performance of the FeSalen electrocatalyts was obtained from the potentials at which reduction steps were observed and from the values of current density obtained by linear sweep voltammetry (LSV) experiments in a cathode half cell, with 6% NO in N$_2$ as gas feed (Fig. 6). The reduction of NO on Pt electrodes in acidic solutions has been extensively investigated by means of voltammetry.[11, 60-66] Previous reports showed that at potentials more positive than ca. -0.31 V vs. Ag/Ag$_2$SO$_4$, N$_2$O and eventually N$_2$ are the only possible products.[65] On the other hand, at potentials more negative than ca. -0.31 vs. Ag/Ag$_2$SO$_4$, NH$_3$ and NH$_2$OH can be formed besides N$_2$O. Therefore, the value of the current density in the region of potential of interest (*i.e.* E$_{cathode}$< -0.31 V vs. Ag/Ag$_2$SO$_4$) can be used as a first indication of the possibility to obtain NH$_2$OH as product of the reduction of NO over the FeSalen electrocatalysts.[8, 19] All the LSV traces of the GDEs prepared using electrocatalysts based on activated carbon show a reduction feature in the most positive region of potential (0.05 V < E$_{cathode}$< 0.3 V vs Ag/Ag$_2$SO$_4$, see Fig. 6.A), which is attributed to surface processes that can take place in this region of

potential such as oxidation-reduction of an adsorbed NO/HNO_2 couple,[67] co-adsorption of SO_4^{2-}, adsorption-desorption of traces of oxygen,[68] or reduction of surface oxygenated groups.[13, 68] Since this peak is less pronounced for the GDE based on pyrolysed FeSalen/AC (Fig. 6.A) and is virtually absent in the GDEs based on electrocatalysts prepared with graphite as support (Fig. 6.B), we ascribe it to the reduction of the oxygenated functional groups present at the surface of untreated activated carbon. The first NO reduction signal over the GDEs based on FeSalen/AC appears between -0.2 and -0.4 V vs. Ag/Ag_2SO_4, which corresponds to the region where the reduction of NO to $[N(H)O]_{ads}$ and its further reduction to NH_2OH are expected to occur.[13, 69] Note that the peak related to the reduction of NO to $[N(H)O]_{ads}$ is observed at -0.1 V vs. Ag/Ag_2SO_4 on the Pt/AC-based GDE (Fig. 6.A).[13, 69] The pyrolysis treatment of the FeSalen/AC led to a poorer LSV performance of the GDE, suggesting that the structure of the complex plays a relevant role in the electrocatalytic behaviour.
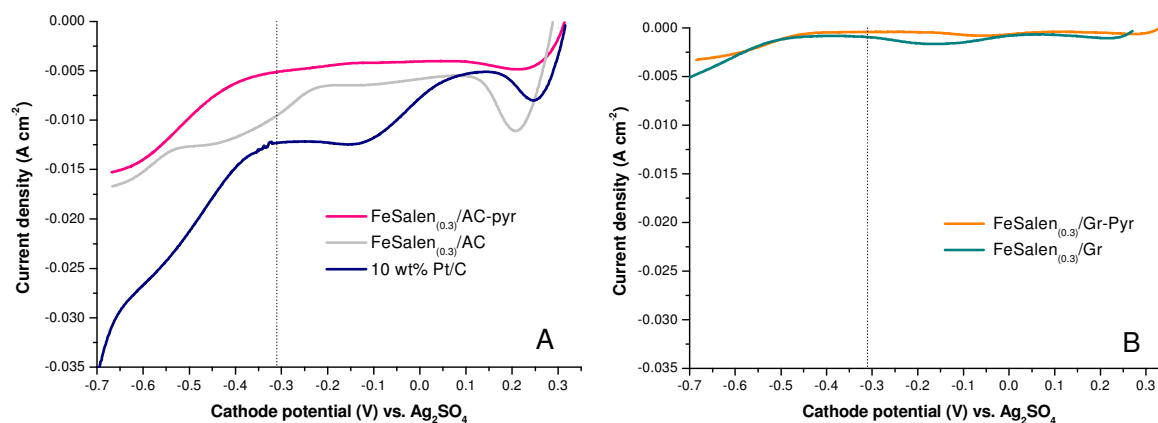

Figure 6. Linear sweep voltammetry of selected cathodes for the reduction of NO (6% NO in the gas feed): (A) cathodes based on the non-pyrolysed and pyrolysed FeSalen$_{(0.3)}$ supported on AC compared to 10 wt% Pt/C; (B) cathodes based on the non-pyrolysed and pyrolysed FeSalen$_{(0.3)}$ supported on graphite. Composition of the active layer of the cathode (working electrode): 10 wt% PTFE and 90 wt% electrocatalyst powder. Geometric projected surface area of this gas diffusion electrode: 10 cm². Reference electrode: Ag/Ag_2SO_4 (0.69 V vs. S.H.E). Counter electrode: Pt-disk welded on a Ti-plate. Electrolyte: 3M aqueous H_2SO_4. Scan rate: 1 mVs^{-1}.

The GDEs prepared using FeSalen supported on graphite showed poor performances compared to their counterparts based on activated carbon (Fig. 6.B), probably due to the low surface area and pore volume of graphite.[70] An additional drawback of graphite for this reaction is its hydrophobicity. Combining PTFE with graphite (both hydrophobic) results in very low hydrophilicity, which would hinder the aqueous electrolyte from reaching the active sites. The high stability and conductivity for which graphite has been often selected as support [14] are not sufficient advantages to counterbalance these drawbacks. Therefore, the development of GDEs based on graphite-supported electrocatalysts was not further pursued in this work. The current densities obtained with the GDEs based on FeSalen/AC electrocatalysts in the region of interest for NH_2OH formation (<-0.31 V vs. Ag/Ag_2SO_4) are much higher than those on the graphite-based GDEs but are still significantly lower compared to the current density obtained with the GDE based on commercial 10 wt% Pt/AC as electrocatalyst (Fig. 6.A), which is consistent with previous reports on NO reduction in a fuel cell.[14] However, it is also known that on Pt-based GDEs, NH_3 (as NH_4^+) rather than NH_2OH (as NH_3OH^+) is the main product for the electroreduction of NO in the region of potential favourable for NH_2OH formation.[71] To complete the evaluation of the FeSalen/AC electrocatalysts, it is important to determine their selectivity towards the desired NH_2OH product. Therefore, the performance of the supported FeSalen electrocatalysts was investigated further in a H_2-NO fuel cell.

3.4 Electrocatalytic performance of the supported Fe-complexes in a H_2-NO fuel cell

The FeSalen/AC materials were evaluated as electrocatalysts for the reduction of NO to NH_2OH by means of chronoamperometric experiments in a H_2-NO fuel cell. Both untreated and pyrolysed FeSalen/AC were studied and their electrocatalytic performance was compared to that of their FePc/AC counterpart, *i.e.* the electrocatalyst that was reported to display the highest selectivity towards NH_2OH so far.[8, 14, 19] The electrocatalytic performance was assessed in terms of current efficiency to NH_2OH [$CE_{NH_2OH}(\%)$] and yield of NH_2OH [$Y_{NH_2OH}(\%)$]. The current efficiency to NH_2OH, *i.e.* the fraction of the generated current that

originates from the reduction of NO to NH_2OH, provides an estimate of the selectivity towards NH_2OH. The yield of hydroxylamine is defined as the percentage of the NO fed to the cathode that was transformed into NH_2OH. It should be noted that the performance of the GDE does not depend only on the intrinsic features of the electrocatalyst but also on other variables related to how the electrocatalyst is integrated in the electrode, which determines its accessibility and degree of utilisation. These features can play a prominent role in the overall process, especially in the region of high current density in which mass transport limitations are determining for electrode polarisation.[11, 72] However, the procedure used to prepare the active layers of the GDEs was the same with all tested electrocatalysts, which implies that the physical features of the electrode (such as the porosity existing between electrocatalyst particles and the effective surface area of the active layer) are expected to be nearly the same irrespective of the type of complex used as electrocatalyst. Indeed, this was confirmed by the very similar surface area of the active layers prepared with either FePc or FeSalen (see Table 2). This means that the results presented in this work allow a meaningful comparison between the electrocatalysts, whereas the influence of the method used for manufacturing the electrode should be taken into account when comparing our results with those from other reports.

A first series of chronoamperometric tests (Table 3) was performed with a relatively low concentration of NO in the cathode feed (6% NO in N_2), as also employed in the LSV study. The GDEs based on AC without any supported metal, either untreated or pyrolysed, showed similar activity in the reduction of NO to NH_2OH (entry 1 and 5 in Table 3), which indicates that the pyrolysis did not have a major effect on the electrocatalytic performance of the activated carbon. In both cases, the current efficiency towards NH_2OH and the yield of NH_2OH were low. The GDE based on $FePc_{(0.3)}$/AC displayed increased activity in the reduction of NO to NH_2OH compared to the parent carbon material, as demonstrated by the higher current density, power density and current efficiency towards NH_2OH. This leads to a much higher hydroxylamine yield (entry 3 in Table 3). The observed high selectivity towards hydroxylamine ($CE_{NH_2OH} = 80\%$) is nicely in agreement with the expectations based on the DFT calculations for experiments carried out employing low NO concentration (see section 3.1). Increasing the metal loading in the electrocatalyst from 0.3 to 3.0 wt.%

resulted in an enhanced reaction rate, as shown by the higher current density and hydroxylamine yield (compare entry 3 to entry 2 in Table 3). However, the increase in metal loading is detrimental for the selectivity towards NH_2OH, since CE_{NH_2OH} decreased from 80% to 55%. This is probably related to the distribution and the proximity of the catalytic sites. At higher metal loading (high concentration of metal complex) there are more active sites close enough to each other as to promote the reaction of two adjacent adsorbed intermediates, leading to the formation of an N-N bond,[7, 9] and the consequent formation of N_2O or N_2 as by-products.

Table 3. Chronoamperometric experiments for the cogeneration of NH_2OH and electricity with various cathode electrocatalysts in a H_2-NO fuel cell (cathode feed: 6% NO in N_2, anode feed: 100% H_2, flow rate of 10 ml min^{-1}, 5 mbar overpressure). The composition of the active layer of the cathode was 10 wt% PTFE and 90 wt% electrocatalyst powder, that of the anode was 15 wt% PTFE and 85 wt% of a commercial Pt-electrocatalyst (10 wt% Pt on activated charcoal type 18, Johnson Matthey). Zirfon® [35] was used as ion-permeable membrane between the electrodes. 3M aqueous H_2SO_4 was used as electrolyte (and was continuously recirculated).

Entry	Electrocatalyst	ΔE_{cell} poised (V)	ΔE_{cell} at steady state^a (V)	Current density (j) at steady state^a (A m^{-2})	Power density at steady state (W m^{-2})	Production rate (mol$_{NH_2OH}$ m^{-2} h^{-1})	CE_{NH_2OH} (%)	Y_{NH_2OH} (%)
1	AC	0	0.004	-56	-0.24	0.07	22	9.2
2	FePc$_{(3.0)}$/AC	0	0.011	-123	-1.29	0.77	55	52
3	FePc$_{(0.3)}$/AC	0	0.010	-76	-0.76	0.60	80	39
4	FeSalen$_{(0.3)}$/AC	0	0.005	-52	-0.26	0.38	51	26
5	AC-pyr	0	0.002	-58	-0.13	0.10	26	14
6	FePc$_{(0.3)}$/AC-pyr	0	0.008	-56	-0.45	0.27	39	18
7	FeSalen$_{(0.3)}$/AC-pyr	0	0.004	-62	-0.22	0.37	54	25

^{a} The values of steady state current density (j) and cell potential (ΔE_{cell}) were recorded after at least 20000 s of experiment (quasi-stationary situation).

The current density, power density and CE_{NH_2OH} attained with the GDE based on FeSalen$_{(0.3)}$/AC are lower than those observed with its counterpart based on FePc$_{(0.3)}$/AC (entry 4 vs. 3 in Table 3). The lower selectivity towards NH$_2$OH observed with FeSalen can be again related to the distance between two neighbouring catalytic active sites: the larger size of the Pc ligand compared to the Salen ligand implies that the minimum distance between neighbouring metal centres will be larger in the case of FePc than in the case of FeSalen, notwithstanding the equal metal loading.

The results with the GDEs based on the pyrolysed electrocatalysts showed that the pyrolysis treatment led to a significant drop in all relevant parameters in the case of FePc$_{(0.3)}$/AC (compare entry 6 with entry 3 in Table 3), whereas the performance of FeSalen$_{(0.3)}$/AC is less affected by the thermal treatment (compare entry 7 with entry 4 in Table 3). As a consequence, the GDE based on FeSalen$_{(0.3)}$/AC-pyr achieved higher current efficiency and yield of NH$_2$OH compared to the GDE based on of FePc$_{(0.3)}$/AC-pyr. The observed trends can be rationalised considering that the pyrolysis treatment leads to partial deterioration of the organic ligands in the complex,[18] which implies that the performance of the pyrolysed electrocatalysts is not anymore influenced by the interaction between the π-delocalised system of the ligand and the metal centre. This interaction is expected to be more relevant in the case of FePc, as the π-delocalised system is much more extended in the Pc ligand compared to the Salen ligand (Fig. 1), thus explaining the more dramatic drop in electrocatalytic performance observed with FePc$_{(0.3)}$/AC-pyr. The deterioration of the Pc ligand would also mean that the role played by this large ligand in distancing the Fe sites on the electrocatalyst surface is diminished, thus accounting for the dramatic decrease in CE_{NH_2OH} observed upon pyrolysis of FePc$_{(0.3)}$/AC (from 80 to 39%, see Table 3).

Table 4. Chronoamperometric experiments for the cogeneration of NH$_2$OH and electricity with various cathode electrocatalysts in a H$_2$-NO fuel cell (cathode feed: 18% NO in N$_2$). Remaining conditions as in the caption of Table 3.

Entry	Electrocatalyst	ΔE_{cell} poised (V)	ΔE_{cell} at steady state[a] (V)	Current density (j) at steady state[a] (A m^{-2})	Power density at steady state (W m^{-2})	Production rate (mol$_{NH_2OH}$ m^{-2} h^{-1})	CE$_{NH_2OH}$ (%)	Y$_{NH_2OH}$ (%)
1	AC	0	0.014	-91.0	-1.3	0.21	18	4.5
2	FePc$_{(0.3)}$/AC	0	0.017	-117	-2.0	0.44	30	9.9
3	FePc$_{(0.3)}$/AC	0.05	0.061	-73.7	-4.5	0.34	42	7.6
4	FePc$_{(0.3)}$/AC	0.10	0.109	-64.2	-7.0	0.32	40	7.1
5	FeSalen$_{(0.3)}$/AC	0	0.016	-106	-1.7	0.53	38	12
6	FeSalen$_{(0.3)}$/AC	0.05	0.063	-86.0	-5.4	0.34	43	7.7
7	FeSalen$_{(0.3)}$/AC	0.10	0.108	-56.0	-6.0	n.d.	n.d	n.d.
8	AC-pyr	0	0.005	-60.1	-0.3	0.19	24	3.9
9	FePc$_{(0.3)}$/AC-pyr	0	0.010	-90.2	-0.9	0.21	18	4.7
10	FePc$_{(0.3)}$/AC-pyr	0.05	0.057	-70.5	-4.0	0.13	15	3.0
11	FePc$_{(0.3)}$/AC-pyr	0.10	0.103	-49.1	-5.1	0.05	8.2	1.1
12	FeSalen$_{(0.3)}$/AC-pyr	0	0.013	-87.3	-1.1	0.21	19	4.7
13	FeSalen$_{(0.3)}$/AC-pyr	0.05	0.062	-77.2	-4.8	0.20	20	4.4
14	FeSalen$_{(0.3)}$/AC-pyr	0.10	0.109	-58.6	-6.4	0.06	8	1.3

[a] The values of steady state current density (j) and cell potential (ΔE_{cell}) were recorded after at least 20000 s of experiment (quasi-stationary situation); n.d.= not detected.

A second series of chronoamperometric tests was performed with 18% NO in N$_2$ as cathode feed (Table 4), which is considered a more suitable feed in view of a prospective industrial application.[4e] The impact of the cell potential was also investigated: the experiments were carried out poising the cell at three different values of cell potential, namely 0 V, 0.05 V and 0.1 V (*i.e.* these are the potentials at which the fuel cell is forced to operate, which would be equivalent to connecting an external circuit with a certain resistance to the cell). In general, the lower the cell potential, the higher the expected NH$_2$OH production rate. Indeed, this trend was observed for each of the tested electrocatalysts (Table 4). Conversely, at very low cell potentials the electrical power output will be close to zero. As a consequence, operation at an intermediate cell

potential (0.05 V in this case, see Table 4) can offer an optimum compromise between power density and NH$_2$OH production. Hence, we selected for comparison the results obtained poising the cell at 0.05 V for GDEs based on FePc$_{(0.3)}$/AC and FeSalen$_{(0.3)}$/AC electrocatalysts (unpyrolysed and pyrolysed). The comparison was based on four performance indicators: current density, power density, current efficiency towards NH$_2$OH and yield of NH$_2$OH (Fig. 7). In previous studies, FePc/AC showed the highest selectivity towards NH$_2$OH production in a NO-H$_2$ fuel cell among various electrocatalysts.[14] When poising the cell at 0.05 V, nearly the same CE$_{NH_2OH}$ and Y$_{NH_2OH}$ were obtained with FePc$_{(0.3)}$/AC and with FeSalen$_{(0.3)}$/AC, whereas current density and power density were higher with the latter. These results show that, with a relatively high NO concentration in the gas feed, FeSalen$_{(0.3)}$/AC is a promising electrocatalyst for the cogeneration of NH$_2$OH and electricity in a NO-H$_2$ fuel cell. The highest yield of NH$_2$OH achieved in the chronoamperometric experiments with 18% NO in N$_2$ as cathode feed was obtained with the GDE based on FeSalen$_{(0.3)}$/AC (12 %, entry 5 in Table 4).

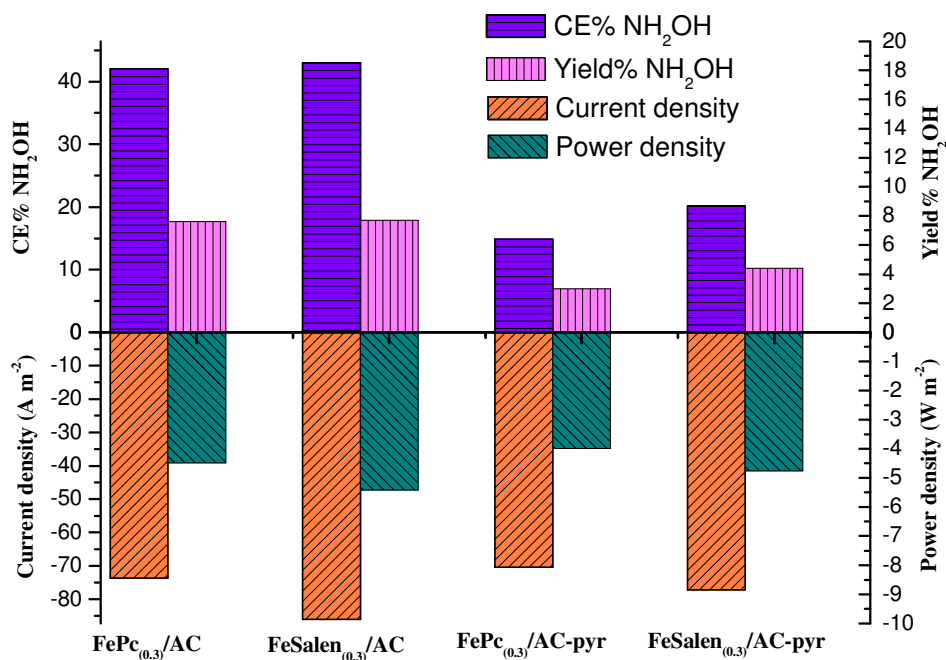**Figure 7**. Electrocatalytic performance of FePc$_{(0.3)}$/AC and FeSalen$_{(0.3)}$/AC electrocatalysts (untreated and pyrolysed) in a single cell poised at 0.05 V cell voltage and with 18% NO gas feed.

The pyrolysis treatment led to a moderate decrease in current density and a more significant drop in CE_{NH_2OH} and, therefore, in Y_{NH_2OH} compared to untreated electrocatalysts, both with $FePc_{(0.3)}$/AC and with $FeSalen_{(0.3)}$/AC (Table 4). Similarly to what was observed for the experiments with the 6% NO feed, the drop in performance was more marked in the case of $FePc_{(0.3)}$/AC-pyr than with $FeSalen_{(0.3)}$/AC-pyr. As a consequence, when comparing $FePc_{(0.3)}$/AC-pyr to $FeSalen_{(0.3)}$/AC-pyr with the cell poised at 0.05 V, the latter exhibited a better electrocatalytic performance based on current and power generation, hydroxylamine production and selectivity (Fig. 7).

When comparing the results of the chronoamperometric tests with 6 and 18% NO in the cathode feed, a general increase in current density and a significant decrease in the current efficiency towards NH_2OH were observed with the higher concentration of NO (Table 3 and 4). The increase in current density is an obvious consequence of the higher amount of NO that reaches the cathode per time unit, although the increase is not linear with NO concentration. This suggests that the reaction rate is not sufficiently high for all NO supplied to the cathode to be consumed, and a higher fraction of NO entering the cathode compartment does not undergo reaction with the 18% NO feed. The observed decrease in CE_{NH_2OH}, and thus in the selectivity towards NH_2OH was predicted based on the DFT study (section 3.1) and is related to the increased probability of an encounter between two NO molecules (or intermediates) when a higher concentration of NO is employed in the feed.[8] Such an encounter is necessary to produce two of the main side-products (N_2O and N_2) of the reduction of NO to NH_2OH (see the reaction scheme in Fig. 2). Based on this analysis, it can also be concluded that the larger distance between neighbouring Fe sites in supported FePc compared to supported FeSalen does not play anymore a significant role in determining the selectivity towards NH_2OH when employing higher NO concentration. This would explain the similar CE_{NH_2OH} values observed for $FePc_{(0.3)}$/AC and $FeSalen_{(0.3)}$/AC with 18% NO (Table 4), whereas $FePc_{(0.3)}$/AC displayed significantly higher CE_{NH_2OH} than $FeSalen_{(0.3)}$/AC with 6% NO in the feed (entries 3 and 4 in Table 3).

3.5 Stability of the electrocatalysts

In this work, the effect of a pyrolysis treatment on the FeSalen/AC and FePc/AC electrocatalysts was investigated because it can strengthen the anchoring of the metal species on the support, thus increasing the stability of the electrocatalyst.[45] On the other hand, this occurs at the expense of the degradation of the organic ligand, resulting in lower activity and selectivity (*vide supra*). In order to investigate whether the pyrolysis treatment led to the expected enhancement in stability, the current density of the GDEs based on FePc$_{(0.3)}$/AC and FeSalen$_{(0.3)}$/AC (untreated and pyrolysed) was plotted as a function of time using the chronoamperometric data obtained in the single cell at 0.05 V with 18% NO gas feed in a 3M H$_2$SO$_4$ solution (Fig. 8). The analysed time interval was between 5000 s (*i.e.* after initial stabilisation) and 85000 s (*i.e.* nearly 24 h). As anticipated, the pyrolysed electrocatalysts displayed better stability under the fuel cell operating conditions compared to the their untreated counterparts, with FePc/AC-pyr showing the smallest deactivation (10% decrease in current density after until 85000 s). It is worth noting that the current density with FePc/AC-pyr showed the smallest decrease but kept decaying during the whole measurement. On the other end, FeSalen/AC-pyr exhibited a larger initial deactivation but then nearly stabilised, showing only ~1% relative current loss between 40000 and 85000 s (Fig. 8). This suggests that FeSalen/AC-pyr contain Fe-species that are less stable and tend to leach rapidly and other ones formed during the pyrolysis that have high stability.
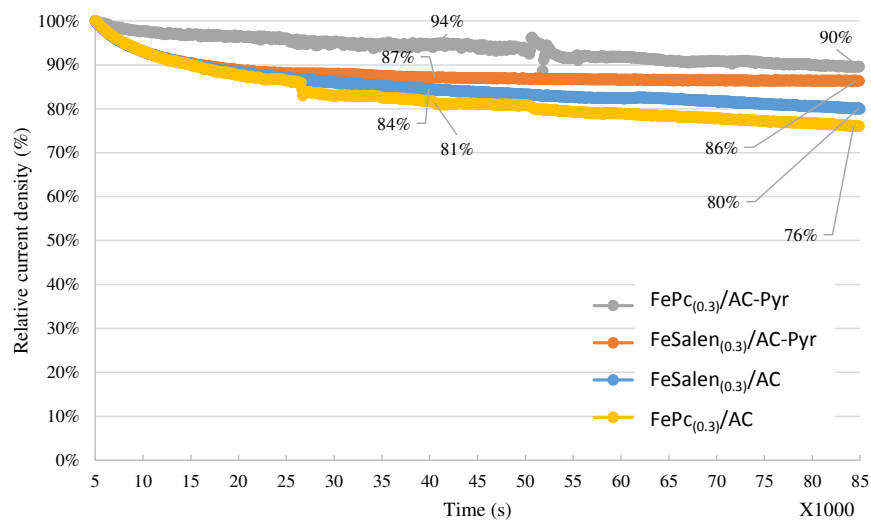
Figure 8. Relative current density vs. time (j–t) plot based on chronoamperometric measurements of the FePc$_{(0.3)}$/AC and FeSalen$_{(0.3)}$/AC (untreated and pyrolysed) electrodes at a cell potential of 0.05 V in a 3 M H$_2$SO$_4$ solution with 18% NO in the gas feed.

The possible tendency of active species to leach from the electrocatalytic material was further investigated by subjecting FePc$_{(0.3)}$/AC and FePc$_{(0.3)}$/AC-pyr to a leaching test in 3M H$_2$SO$_4$, *i.e.* in a similar environment as that in which the electrochemical tests were performed. In agreement with the chronoamperometirc results, the pyrolysed material displayed higher stability against leaching of Fe species compared to the untreated materials (Table 5). However, also the pyrolysed material experienced a significant leaching of Fe upon treatment with the strongly acidic solution (50% loss after 52 h). In line with this result, a substantial decrease in Fe-content was detected as well in the case of the GDE prepared using FePc$_{(0.3)}$/AC-pyr (61% after 130 h of operation in the fuel cell, see Table 7). These results indicate that the pyrolysis treatment mitigates leaching of the metal, but does not completely supress it. Remarkably, the leaching degree from the pyrolysed material increased very little when prolonging the length of the acid treatment (50% after 52 h, 57% after 168 h), supporting the hypothesis that some of the Fe-species are sufficiently stabilised by the pyrolysis treatment whereas others still tend to leach out. Possible strategies to

29

mitigate further the issues with leaching include an optimisation of the pyrolysis treatment (time, temperature) and of the GDE composition. Substituting the concentrated sulphuric acid used so far with a milder electrolyte could also be considered as an approach to tackle this problem in future research.

Table 5. Stability test for pyrolysed and unpyrolysed $FePc_{(0.3)}/AC$ electrocatalysts in 3M aqueous H_2SO_4.

Entry	Sample	Time	Initial Fe content (wt.%)	Final Fe content (wt.%)	Fe leaching (%)
1	$FePc_{(0.3)}/AC$ (electrocatalyst powder)	52 h	0.32 [a]	0.08 [a]	75
2	$FePc_{(0.3)}/AC$-pyr (electrocatalyst powder)	52 h	0.28 [a]	0.14 [a]	50
3	$FePc_{(0.3)}/AC$-pyr (electrocatalyst powder)	168 h	0.28 [a]	0.12 [a]	57
4	$FePc_{(0.3)}/AC$-pyr (GDE)	130 h	0.31 [b]	0.12 [b]	61

[a] Measured by ICP-OES; [b] measured by XRF.

4. Conclusions

FeSalen complexes supported on activated carbon are reported here for the first time as electrocatalysts for the reduction of NO to NH_2OH with cogeneration of electricity. The gas diffusion electrodes prepared using FeSalen complexes supported on activated carbon displayed comparable yet slightly enhanced performance relative to the reference FePc/AC electrocatalysts when operating with a higher NO concentration (18%), whereas they were inferior at lower NO concentration (6%) in the feed. If the electrocatalysts were pyrolysed, the electrodes based on FeSalen/AC were superior to those based on FePc/AC in terms of current and power generation, hydroxylamine production and selectivity. The pyrolysis treatment was introduced to increase the stability of the electrocatalyst. Indeed, the pyrolysed FeSalen/AC, though showing inferior electrocatalytic performance compared to its untreated counterpart, displayed higher stability under fuel cell operating conditions by maintaining almost constant current density after an initial

slight deactivation. The experimental work was complemented by a DFT study of the reaction mechanism, which provided a useful support for explaining the observed decrease in selectivity towards hydroxylamine upon increase in the concentration of NO in the gas feed. Finally, the Salen ligand is significantly less expensive than phthalocyanine (Pc) and the FeSalen complex can be prepared with a straightforward, high-yield (typically above 80%) method. These are important assets from the point of view of the feasibility of a potential industrial production.

Supporting Information

Experimental details about the synthesis of FeSalen and about the electrochemical tests. Table with relative energies of low-lying spin states in all intermediate. Table of atomic coordinates. Figure showing the spin density of FePor-N(H)OH ($S = 1/2$) and FePor-NH$_2$ ($S = 1/2$).

References

[1] B. Raton, CRC Handbook of Chemistry and Physics (87th ed.), CRC Press, 2006.

[2] S. Polizzi, A. Benedetti, G. Fagherazzi, C. Goatin, R. Strozzi, G. Talamini, L. Toniolo, J. Catal., 106 (1987) 494-499.

[3] W. Lewdorowicz, W. Tokarz, P. Piela, P.K. Wrona, J. New Mat. Electrochem. Systems, 9 (2006) 339-343.

[4] X. Sheng, B. Wouters, T. Breugelmans, A. Hubin, I.F.J. Vankelecom, P.P. Pescarmona, Appl. Catal. B: Environ. , 147 (2014) 330-339.

[5] X. Sheng, B. Wouters, T. Breugelmans, A. Hubin, I.F.J. Vankelecom, P.P. Pescarmona, Chemelectrochem, 1 (2014) 1198-1210.

[6] B. Wouters, X. Sheng, A. Boschin, T. Breugelmans, E. Ahlberg, I.F.J. Vankelecom, P.P. Pescarmona, A. Hubin, Electrochim. Acta, 111 (2013) 405-410.

[7] X. Sheng, N. Daems, B. Geboes, M. Kurttepeli, S. Bals, T. Breugelmans, A. Hubin, I.F.J. Vankelecom, P.P. Pescarmona, Appl. Catal. B: Environ. , 176 (2015) 212-224.

[8] N. Daems, X. Sheng, Y. Alvarez-Gallego, I.F.J. Vankelecom, P.P. Pescarmona, Green Chem. , 18 (2016) 1547-1559.

[9] S.H. Langer, K.T. Pate, Nature, 284 (1980) 434-435.

[10] M.J. Foral, S.H. Langer, Electrochim. Acta 36 (1991) 299-307.

[11] I. Paseka, J. Voňková, Electrochim. Acta 25 (1980) 1251-1253.

[12] K. Hara, M. Kamata, N. Sonoyama, T. Sakata, Journal of Electroanalytical Chemistry, 451 (1998) 181-186.

[13] J.A. Colucci, M.J. Foral, S.H. Langer, Electrochim. Acta, 30 (1985) 1675-1685.

[14] K. Otsuka, H. Sawada, I. Yamanaka, J. Electrochem. Soc., 143 (1996) 3491-3497.

[15] M.T. de Groot, M. Merkx, A.H. Wonders, M.T.M. Koper, J. Am. Chem. Soc., 127 (2005) 7579-7586.

[16] A. Daiber, T. Nauser, N. Takaya, T. Kudo, P. Weber, C. Hultschig, H. Shoun, V. Ullrich, J. Inorg. Biochem., 88 (2002) 343-352.

[17] J.K. Nørskov, J. Rossmeisl, A. Logadottir, L. Lindqvist, J.R. Kitchin, T. Bligaard, H. Jonsson, J. Phys. Chem. B, 108 (2004) 17886-17892.

[18] I. Herrmann, U.I. Kramm, J. Radnik, S. Fiechter, P. Bogdanoff, J. Electrochem. Soc. , 156 (2009) B1283-B1292.

[19] Y. Alvarez-Gallego, X. Dominguez-Benetton, D. Pant, L. Diels, K. Vanbroekhoven, I. Genné, P. Vermeiren, Electrochim. Acta, 82 (2012) 415-426.

[20] P.J. Farmer, F. Sulc, J. Inorg. Biochem. , 99 (2005) 166-184.

[21] J.P. Perdew, W. Yue, Phys. Rev. B, 33 (1986) 8800-8802.

[22] S.M. Lui, W. Liang, A. Soriano, J.A. Cowan, J. Am. Chem. Soc. , 116 (1994) 4531-4536.

[23] O. Einsle, A. Messerschmidt, R. Huber, P.M.H. Kroneck, F. Neese, J. Am. Chem. Soc., 124 (2002) 11737-11745.

[24] R. Silaghi-Dumitrescu, Eur. J. Inorg. Chem. , (2003) 1048-1052.

[25] R. Ahlrichs, M. Bär, M. Häser, H. Horn, C. Kolmel, C. Chem. Phys. Lett. , 162 (1989) 165-169.

[26] A.D. Becke, Phys. Rev. A 38 (1988) 3098-3100.

[27] S. Grimme, J. Comput. Chem. , 27 (2006) 1787-1799.

[28] F. Weigend, R. Ahlrichs, Phys. Chem. Chem. Phys. , 7 (2005) 3297-3305.

[29] P.E.M. Siegbahn, M.R.A. Blomberg, S.-L. Chen, J. Chem. Theory Comput. , 6 (2010) 2040-2044.

[30] G.S. Karlberg, J. Rossmeisl, J.K. Nørskov, Phys. Chem. Chem. Phys. , 9 (2007) 5158-5161.

[31] A. Rauf, A. Shah, K.S. Munawar, A.A. Khan, R. Abbasi, M.A. Yameen, A.M. Khan, A.R. Khan, I.Z. Qureshi, H.B. Kraatz, R. Zia ur, J. Mol. Struct., 1145 (2017) 132-140.

[32] H.A.R. Pramanik, S. Chanda, C.R. Bhattacharjee, P.C. Paul, P. Mondal, S.K. Prasad, D.S.S. Rao, Liquid Crystals, 43 (2016) 1606-1615.

[33] R. Chen, H. Li, D. Chu, G. Wang, J. Phys. Chem. C, 113 (2009) 20689-20697.

[34] C. Carkeet, S.R. Dueker, J.R. Follett, T.E. Correa, A.J. Clifford, Faseb Journal, 15 (2001) A260-A260.

[35] P.H. Vermeiren, R. Leysen, H. Beckers, J.P. Moreels, A. Claes, J. Porous Mater., 15 (2008) 259-264.

[36] S.T. Seger, P. Rydberg, L. Olsen, Chem. Res. Toxicol., 28 (2015) 597-603.

[37] S. Vancoillie, H. Zhao, T. Van Tan, M.F.A. Hendrickx, K. Pierloot, J. Chem. Theory Comput., 7 (2011) 3961-3977.

[38] J.A. McCleverty, Chemical Reviews, 104 (2004) 403-418.

[39] K.R. Sawyer, R.P. Steele, E.A. Glascoe, J.F. Cahoon, J.P. Schlegel, M. Head-Gordon, C.B. Harris, J. Phys. Chem. A 112 (2008) 8505-8514.

[40] M.L. Fernández, D.A. Estrin, S.E. Bari, J. Inorg. Biochem., 102 (2008) 1523-1530.

[41] J. Li, S. Li, Phys. Chem. Chem. Phys. , 9 (2007) 3304-3311.

[42] D. Sun, W.F. Schneider, J.B. Adams, D. Sengupta, J. Phys. Chem. A 108 (2004) 9365-9374.

[43] P. Kalugasalam, S. Ganesan, IJEST, 2 (2010) 2574-2579.

[44] R. Seoudi, G.S. El-Bahy, Z.A. El Sayed, J. Mol. Struct. , 753 (2005) 119-126.

[45] A. Ahmad, R.A. Collins, J. Phys. D: Appl. Phys., 24 (1991) 1894-1897.

[46] M.M. Rahman, S.H. Samsuddin, M.F. Miskon, K. Yunus, A.M. Yusof, Green Chem Lett Rev, 8 (2015) 9-20.

[47] L.J. Liu, H.M. Guo, B. Xue, H. Lou, M. Chen, RSC Adv., 5 (2015) 66704-66710.

[48] C. Moreno-Castilla, M.A. Ferro-Garcia, J.P. Joly, I. Bautista-Toledo, F. Carrasco-Marin, J. Rivera-Utrilla, Langmuir, 11 (1995) 4386-4392.

[49] L. Ohlin, P. Bazin, F. Thibault-Starzyk, J. Hedlund, M. Grahn, J. Phys. Chem. C, 117 (2013) 16972-16982.

[50] S. Baranton, C. Coutanceau, E. Garnier, J.M. Léger, J. Electroanal. Chem, 590 (2006) 100-110.

[51] G. Wu, C.M. Johnston, N.H. Mack, K. Artyushkova, M. Ferrandon, M. Nelson, J.S. Lezama-Pacheco, S.D. Conradson, K.L. More, D.J. Myers, P. Zelenay, J. Mater. Chem, 21 (2011) 11392-11405.

[52] B. Smith, Infrared Spectral Interpretation: A Systematic Approach, CRC, 1998.

[53] A. Sheelam, K. Ramanujam, Electrochim. Acta 216 (2016) 457-466.

[54] D.S.R. Rubavathi, S. Balakumar, Asian J. Chem., 22 (2010) 4891-4897.

[55] K.K. Bania, D. Bharali, B. Viswanathan, R.C. Deka, Inorg. Chem., 51 (2012) 1657-1674.

[56] E. Kadwa, H.B. Friedrich, M.D. Bala, Inorg. Chim. Acta., 463 (2017) 112-117.

[57] A.A. Khandar, K. Nejati, Z. Rezvani, Molecules, 10 (2005) 302-311.

[58] N. Daems, X. Sheng, I.F.J. Vankelecom, P.P. Pescarmona, J. Mater. Chem. A, 2 (2014) 4085-4110.

[59] M. Gonçalves, M. Molina-Sabio, F. Rodriguez-Reinoso, J Anal Appl Pyrolysis. , 89 (2010) 17-21.

[60] B.G. Snider, D.C. Johnson, Anal. Chim. Acta, 105 (1979) 9-23.

[61] A.C.A. de Vooys, M.T.M. Koper, R.A. van Santen, J.A.R. van Veen, J. Catal., 202 (2001) 387-394.

[62] A.C.A. de Vooys, M.T.M. Koper, R.A. van Santen, J.A.R. van Veen, Electrochim. Acta., 46 (2001) 923-930.

[63] A.C.A. de Vooys, G.L. Beltramo, B. van Riet, J.A.R. van Veen, M.T.M. Koper, Electrochim. Acta., 49 (2004) 1307-1314.

[64] E. Casero, C. Alonso, J.A. Martin-Gago, F. Borgatti, R. Felici, F. Renner, T.L. Lee, J. Zegenhagen, Surf. Sci, 507 (2002) 688-694.

[65] L.J.J. Janssen, M.M.J. Pieterse, E. Barendrecht, Electrochim. Acta 22 (1977) 27-30.

[66] J.F. van der Plas, E. Barendrecht, Rec. Trav. Chem. Pays-Bas, 96 (1977) 133-136.

[67] G.L. Beltramo, M.T.M. Koper, Langmuir, 19 (2003) 8907-8915.

[68] J.F. van der Plas, E. Barendrecht, Rec. Trav. Chem. Pays-Bas, 97 (1978) 65-69.

[69] J.A. Colucci, M.J. Foral, S.H. Langer, Electrochim. Acta, 30 (1985) 521-528.

[70] A.L. Dicks, J. Power Sources 156 (2006) 128-141.

[71] M.J. Foral, S.H. Langer, Electrochim. Acta 33 (1988) 257-263.

[72] P. Gouérec, L. Poletto, J. Denizot, E. Sánchez-Cortejón, J.H. Miners, J. Power Sources 129 (2004) 193-204.